Optics Letters

Ultrasensitive refractometer based on helical long-period fiber grating near the dispersion turning point

Shen Liu,[1] Min Zhou,[1,2] Zhe Zhang,[1] Zhongyuan Sun,[1] Zhiyong Bai,[1,*] and Yiping Wang[1]

[1]Key Laboratory of Optoelectronic Devices and Systems of Ministry of Education/Guangdong Province, College of Physics and Optoelectronic Engineering, Shenzhen University, Shenzhen 518060, China
[2]The School of Communication and Information Engineering, Chongqing University of Posts and Telecommunications, Chongqing, 400065, China
*Corresponding author: baizhiyong@szu.edu.cn

Received 28 February 2022; revised 18 April 2022; accepted 20 April 2022; posted 25 April 2022; published 13 May 2022

Precise and accurate measurements of the optical refractive index (RI) for liquids are increasingly finding applications in biochemistry and biomedicine. Here, we demonstrate a dual-resonance helical long-period fiber grating (HLPFG) near the dispersion turning point (DTP), which exhibits an ultrahigh RI sensitivity (~25546 nm/RIU at ~1.440). The achieved RI sensitivity is, to the best of our knowledge, more than one order of magnitude higher than a conventional HLPFG. The ultrahigh RI sensitivity can improve the RI measurement precision and accuracy significantly. Furthermore, ultralow wavelength shifts (nearly zero) with temperature and strain ranging from 20 to 100°C and 0 to 2226 με, respectively, are also demonstrated for the proposed HLPFG, which may be a good candidate for developing new low-cross-talk sensors.

https://doi.org/10.1364/OL.456571

As one of the most fundamental physical parameters, optical refractive index (RI) determination with high precision and accuracy is of great importance in environment monitoring, chemical analysis [1,2], biological detection [3], medical diagnosis [4], as well as environment monitoring [5]. Over the past decades, fiber-optic RI sensors have been widely investigated and applied owing to their intriguing characteristics, such as small size, high sensitivity, and *in vivo* sensing abilities [6–8]. Tremendous sensing schemas, such as the fiber Bragg gratings (FBGs) [9,10], tilt fiber Bragg gratings (TFBGs) [11,12], long-period fiber gratings (LPFGs) [13,14], and other interferometric and [15–20] surface plasmon resonance (SPR) sensors [21–23] for RI determination have been well developed and each of them exhibits its own advantages and limitations. For example, FBGs and conventional LPFGs exhibit convenience in preparation but with low RI sensitivities (hundreds and thousands of nanometers per RIU, respectively) [9–14]. Despite the RI sensitivity of a fiber-SPR sensor being improved to 22779 nm/RIU at RI of ~1.335 by employing a low-RI polymer fiber substrate, it needs not only the special fibers but careful polishing, followed by metal coatings on the fiber.

Cladding-mode dual resonance at the dispersion turning points (DTPs) of the modes for an LPFG was first theoretically demonstrated by Shu *et al.* in 2002 [24,25], where they predicted its potential for use as ultrasensitive sensors. However, in their experiments, where an LPFG inscribed by UV exposure on a B–Ge co-doped fiber is employed, the wavelength changes only −164.8 nm for an RI changing from 1 to 1.44, which can be attributed to both the fiber material and the order of the cladding mode that is employed. Moreover, only within a temperature range of 0–10°C, the mode exhibits a single resonance that is wavelength-independent of temperature, meaning that the cross talk of temperature to RI is remarkable. After its first demonstration, a lot of impressive works on RI sensing based on LPFGs at DTP have been reported [26–31]. However, for LPFGs without a complicated sensitization coating or special optical fibers [26,27], the highest RI sensitivity experimentally achieved is 13,497.7 nm/RIU in the RI range of 1.447–1.453 [30], which also exhibits a temperature response (temperature–RI cross talk) of 0.77 nm/°C.

In this work, we propose a dual-resonance helical long-period fiber grating (HLPFG) inscribed at the DTP, which exhibits simultaneously an ultrahigh RI sensitivity (25546 nm/RIU at an RI of ~1.440) and ultralow wavelength shift (nearly zero) for temperature or strain variations from 20 to 100°C and 0 to 2226 με, respectively.

As discussed in [24,25], higher order cladding modes resonance may exhibit dual resonances, which exhibits higher sensitivities. As such, we first numerically simulate the dispersion curvature of the fundamental and high-order cladding modes ($LP_{1,9}$, $LP_{1,10}$, and $LP_{1,11}$) of a conventional single-mode fiber (SMF-28), using COMSOL Multiphysics. The parameters values in our simulation are a core diameter of 8.2 μm, cladding diameter of 125 μm, and the RI dispersion of the silica cladding and Ge-doped core are calculated using Sellmeier equations. The results are plotted and shown in Fig. 1(a). It is well known that the resonance wavelength λ_{res} of an LPFG with a period Λ can be determined by the phase-matching condition [24,33]:

$$\lambda_{res} = (n_{co}^{eff} - n_{cl}^{eff})\,\Lambda, \tag{1}$$

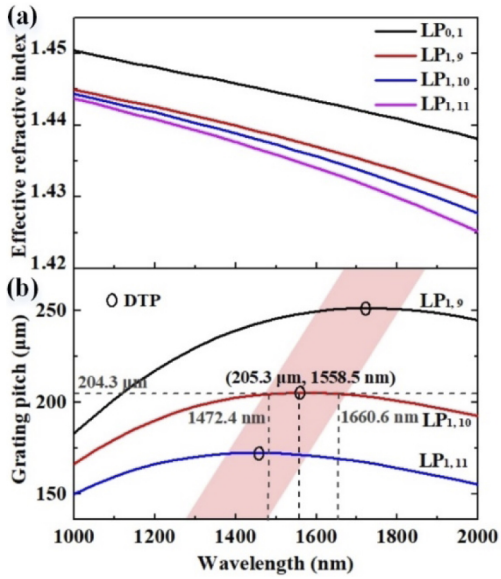

Fig. 1. (a) Simulated dispersion curves of the fundamental core mode and high-order cladding modes ($LP_{1,9}$, $LP_{1,10}$, and $LP_{1,11}$) of SMF-28 using COMSOL Multiphysics; (b) calculated resonant wavelength of the three cladding modes versus grating period according to Eq. (1) and Fig. 1(a).

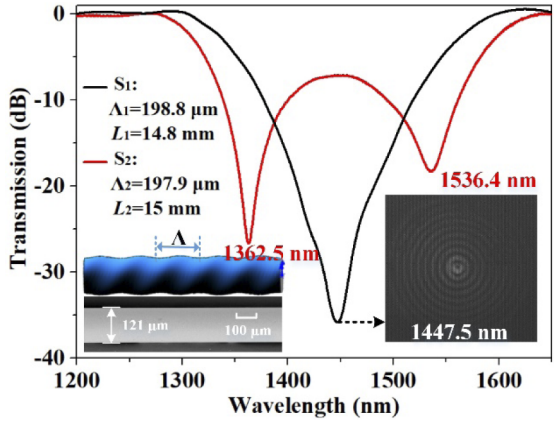

Fig. 2. Transmission spectra of two representative HLPFGs. Insets: schematic of the helical modulation and scanning electron microscopy (SEM) image of one prepared HLPFG (S_1).

where n_{co}^{eff} and n_{cl}^{eff} are the effective indexes of the fundamental core mode and the cladding mode, respectively. The mode dispersion curves are calculated and shown in Fig. 1(a). By inputting the obtained effective RIs into Eq. (1), the resonant wavelength of the three cladding modes ($LP_{1,9}$, $LP_{1,10}$, and $LP_{1,11}$) versus the grating period are calculated and plotted in Fig. 1(b). The open circles in Fig. 1(b) represent the dispersion turning points (DTPs) of the three cladding modes (i.e., the corresponding grating pitch and resonant wavelength of $LP_{1,10}$ are approximately 205.3 μm and 1558.5 nm, respectively). When the grating period is a little smaller than that of the DTPs, for each cladding mode, there exists two resonant wavelengths (the so-called dual resonance, i.e., when the grating pitch is 204.3 μm, the corresponding resonant wavelengths of $LP_{1,10}$ are approximately 1472.4 nm and 1660.6 nm, respectively). As theory predicts, when the grating period is at or near the DTP, as shown in the shadow area of Fig. 1(b), high sensitivity can be achieved for the LPFG.

In the experiments, we employ a modified oxyhydrogen-flame tapering setup with a fiber rotating at high speed to inscribe an HLPFG. The setup and the mechanism for LPFG formation have been detailed in our previous works [32,33]. Several HLPFGs with different grating periods are prepared, and the transmission spectra of two representative HLPFGs [i.e., at the DTP (S_1) and near the DTP (S_2)] are shown in Fig. 2, where the resonant peak is identified as the $LP_{1,10}$ by the CCD image, as show in the inset of Fig. 2. The grating periods are 198.8 μm and 197.9 μm with grating lengths of $L_1 = 14.8$ mm and $L_2 = 15$ mm, respectively. The resonant wavelength and coupling strength of S_1 are 1447.5 nm and −35.9 dB, respectively. Both the grating pitch Λ and resonant wavelength of the experiments exhibit a deviation from the calculated results shown in Fig. 1(b), which can be attributed to the thinning of the fiber [33]. The insets in Fig. 2 also schematically illustrate the helical modulation and the scanning electron microscopy (SEM) image of the prepared HLPFG (S_1). The measured outer diameter of S_1 (121 μm) is a little smaller than that of the standard SMF-28 (125 μm), which is due to a preset certain velocity difference of two translation stages to keep the fiber straight [33].

Following the HLPFG preparation, experiments are carried out to characterize the sensing performance of the proposed HLPFG at DTP (S_1). RI response of the HLPFG is first investigated by tracking the resonant peak when immersing the HLPFG in a series of RI liquids (CargilleLabs) with RI ranging from 1.310 to 1.442 at room temperature (25°C). The transmission spectrum evolution is recorded by an optical spectrum analyzer (OSA) and plotted in Fig. 3(a), where the resonant mode ($LP_{1,10}$) exhibits a single peak in air, and quickly bifurcates into two peaks with the surrounding RI increase. The rate of the peak separation rises rapidly with the increase of RI. Quantitative characterization of the RI response is then carried out and shown in Fig. 3(b). The blueshifted resonant peak (dip 1) is less sensitive than its redshifted counterpart (dip 2), (the RI sensitivities at RI of ~1.440 are approximately −2564 nm/RIU and 22982 nm/RIU for dip 1 and dip 2, respectively). This difference is due to the RI sensitivity of the resonant wavelength exhibiting a λ^4 dependence [24]. By counting the wavelength separation of the two resonant dips, an ultrahigh RI sensitivity of ~25546 nm/RIU is obtained, which is, to the best of our knowledge, more than one order of magnitude higher than that of the conventional HLPFG [34]. This can be understood by the expression of RI sensitivity:

$$\frac{d\lambda_{res}}{dn_{sur}} = \frac{d\lambda_{res-long}}{dn_{sur}} - \frac{d\lambda_{res-short}}{dn_{sur}}, \tag{2}$$

where $\lambda_{res-long}$ and $\lambda_{res-short}$ are the resonant wavelength of dip 1 and dip 2, respectively. The wavelength shift of the two dips with RI change can be calculated by [24]

$$\frac{d\lambda_{res-}}{dn_{sur}} = \lambda_{res-} \cdot \gamma \cdot \Gamma_{sur}, \tag{3}$$

where γ and Γ_{sur} are the waveguide dispersion factor and sensitivity factor to the surrounding RI, respectively.

Compared with the conventional HLPFG, our HLPFG near the DTP has a larger waveguide dispersion factor γ and RI sensitivity factor Γ_{sur} [24]. Moreover, the RI sensitivity in our experiment is obtained by counting the wavelength separation

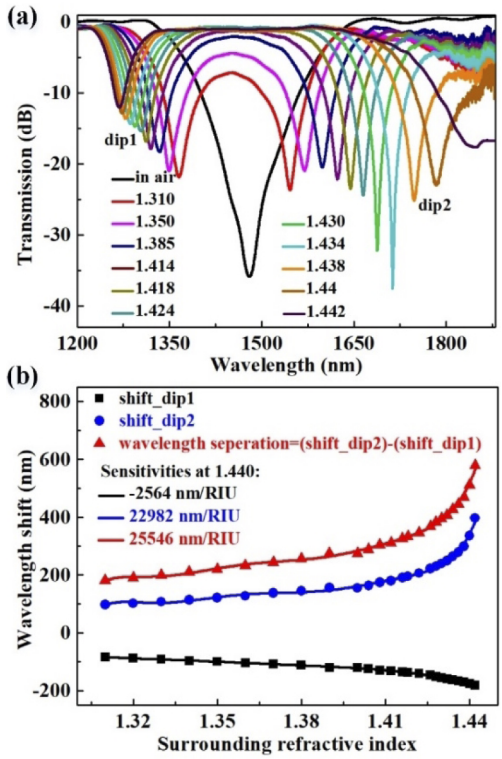

Fig. 3. RI response of the HLPFG at DTP (S_1): (a) transmission spectrum evolution with surrounding RI; (b) resonant wavelength versus surrounding refractive index.

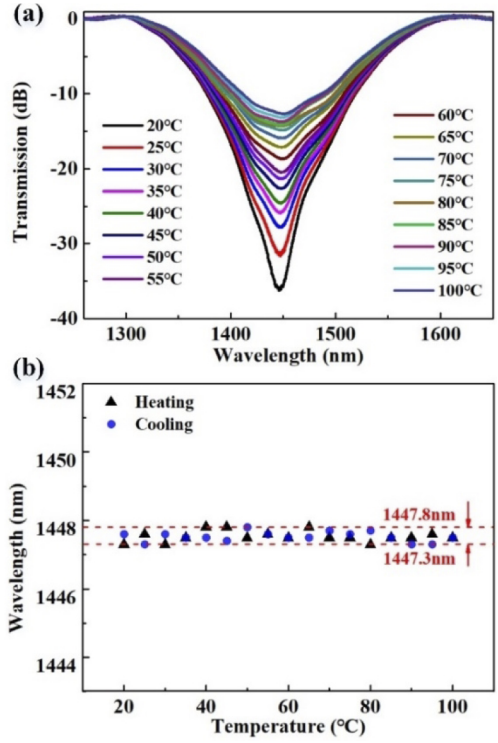

Fig. 4. Temperature responses of the HLPFG at DTP (S_1): (a) transmission spectra evolution with temperature; (b) resonant wavelength versus temperature.

of the two resonant dips, which improve the sensitivity further. Altogether, an ultrahigh RI sensitivity is obtained.

Temperature and strain responses of the HLPFG (S_1) are also investigated. Figure 4(a) illustrates the transmission spectrum evolution with temperature increasing from 20 to 100°C in steps of 5°C, and Fig. 4(b) shows the resonant wavelength versus temperature. Within the temperature range of 20–100°C, the resonant wavelength hardly changes, while the resonant strength decreases significantly with the increase of temperature. This phenomenon agrees well with the fact that for LPFGs designed to operate at the DTP but a little off resonance, external perturbations induce only a variation in the coupling efficiency, and the maximum coupling wavelength remains constant [24]. The strain response of the HLPFG (S_1) has been measured by the same setup detailed in our previous work [32]. The total length of the stretched fiber, including the single-mode fiber and HLPFG, is 12.6 cm. As shown in Fig. 5, the evolution of the transmission spectrum and the resonant wavelength are recorded, while a tension strain increasing from 0 to 2226 με in steps of 159 με is applied to the HLPFG (S_1). A similar phenomenon has been found where the increasing strain decreases the coupling strength without a detectable change in resonant wavelength.

The total wavelength fluctuation of the resonant dip for both the temperature test from 20 to 100°C and the tension strain test from 0 to 2226 με are at most ±0.3 nm. The shifts of the wavelength can be attributed to the noise of the employed OSA, as well as the air RI fluctuation. It is worth noting that the strength change of the resonant peak with temperature or tension strain can also be developed for sensing by using the intensity demodulation approach.

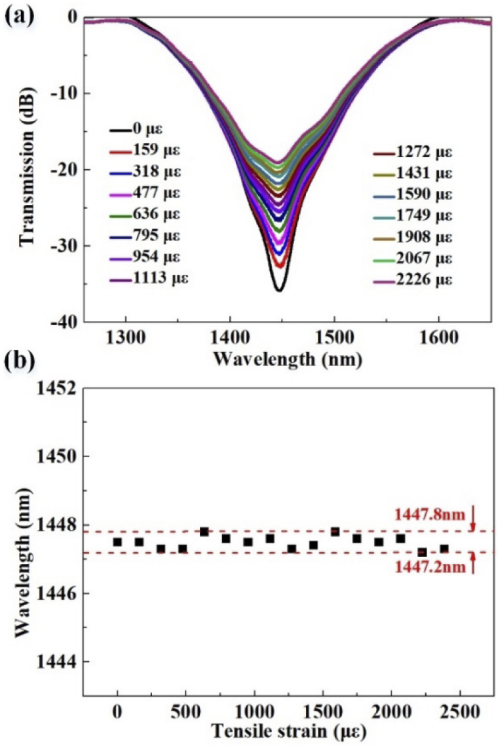

Fig. 5. Strain responses of the HLPFG at DTP (S_1): (a) transmission spectra evolution with tension strain; (b) resonant wavelength versus tension strain.

In conclusion, we propose and experimentally demonstrate an ultrasensitive (~25546 nm/RIU at ~1.440) refractometer based on an HLPFG at the DTP. The achieved sensitivity is more than one order of magnitude higher than that of conventional HLPFGs, which may improve the precision and accuracy of RI measurements significantly. An ultralow wavelength shift of the HLPFG to temperatures and strains in the ranges of 20–100°C and 0–2226 με, respectively, are also a new experimental finding, which may be promising in developing new low-cross-talk sensors.

Funding. National Natural Science Foundation of China (61905164, 61905165, 62175165); Basic and Applied Basic Research Foundation of Guangdong Province (2018KQNCX219, 2021A1515011834); Shenzhen Science and Technology Innovation Program (JCYJ20210324120403009, RCBS20200714114922296).

Disclosures. The authors declare no conflicts of interest.

Data availability. Data underlying the results presented in this paper are not publicly available at this time but may be obtained from the authors upon reasonable request.

REFERENCES

1. J. Villatoro, M. P. Kreuzer, R. Jha, V. P. Minkovich, V. Finazzi, G. Badenes, and V. Pruneri, Opt. Express **17**, 1447 (2009).
2. C. Elosua, I. Matias, C. Bariain, and F. J. Arregui, Sensors **6**, 1440 (2006).
3. F. Chiavaioli, P. Zubiate, I. D. Villar, C,R Zamarreño, A. Giannetti, S. Tombelli, C. Trono, F. J. Arregui, I. R. Matias, and F. Baldini, ACS Sens. **3**, 936 (2018).
4. S. Shabahang, S. Kim, and S. H. Yun, Adv. Funct. Mater. **28**, 1706635 (2018).
5. F. Esposito, A. Zotti, G. Palumbo, S. Zuppolini, M. Consales, A. Cutolo, A. Borriello, S. Campopiano, M. Zarrelli, A. Iadicicco, F. Esposito, A. Zotti, G. Palumbo, S. Zuppolini, M. Consales, A. Cutolo, A. Borriello, S. Campopiano, and M. Zarrelli, Sensors **18**, 1435 (2018).
6. X. D. Wang and O. S. Wolfbeis, Anal. Chem. **88**, 203 (2016).
7. Y. Zhao, X. G. Hu, S. Hu, and Y. Peng, Biosens. Bioelectron. **166**, 112447 (2020).
8. Z. Zhang, Y. Y. Wang, M. Zhou, J. He, C. R. Liao, and Y. P. Wang, Chin. Opt. Lett. **19**, 070601 (2021).
9. C. P. Lin, C. R. Liao, J. Wang, J. He, Y. Wang, Z. Y. Li, T. H. Yang, F. Zhu, K. M. Yang, Z. Zhang, and Y. P. Wang, Opt. Lett. **42**, 1684 (2017).
10. J. Wang, C. P. Lin, C. R. Liao, Z. S. Gan, Z. Y. Li, S. Liu, L. Xu, Y. Wang, J. He, and Y. P. Wang, Opt. Express **26**, 3732 (2018).
11. Y. C. Lu, R. Geng, C. C. Wang, F. Zhang, C. Liu, T. G. Ning, and S. S. Jian, J. Lightwave Technol. **28**, 1677 (2010).
12. X. H. Hu, C. F. Jeff Pun, H. Y. Tam, P. Mégret, and C. Caucheteur, Opt. Lett. **39**, 6835 (2014).
13. G. L. Yin, Y. P. Wang, C. R. Liao, B. Sun, Y. J. Liu, S. Liu, Q. Wang, K. M. Yang, J. Tang, and X. Y. Zhong, IEEE Photonics Technol. Lett. **27**, 375 (2015).
14. J. Yang, L. Yang, C. Q. Xu, and Y. F. Li, J. Lightwave Technol. **25**, 372 (2007).
15. Z. Zhang, J. He, B. Du, K. K. Guo, and Y. P. Wang, Opt. Express **27**, 29649 (2019).
16. H. L. Zhang, F. Zhang, B. T. Cong, and Y. F. Qi, Optoelectron. Lett. **17**, 513 (2021).
17. C. Y. Li, B. B. Song, J. X. Wu, W. Huang, X. J. Wu, and C. Jin, Optoelectron. Lett. **17**, 193 (2021).
18. Z. Zhang, J. He, B. Du, F. C. Zhang, K. K. Guo, and Y. P. Wang, Opt. Lett. **43**, 6009 (2018).
19. Z. Zhang, J. He, Q. Dong, Z. Y. Bai, C. R. Liao, Y. Wang, S. Liu, K. K. Guo, and Y. P. Wang, Opt. Lett. **43**, 3017 (2018).
20. Z. Zhang, C. R. Liao, J. Tang, Z. Y. Bai, K. K. Guo, M. X. Hou, J. He, Y. Wang, S. Liu, F. Zhang, and Y. P. Wang, J. Lightwave Technol. **35**, 18 (2017).
21. Z. W. Ding, T. T. Lang, Y. Wang, and C. L. Zhao, J. Lightwave Technol. **35**, 21 (2017).
22. J. Zhao, S. Q. Cao, C. R. Liao, Y. Wang, G. J. Wang, X. Z. Xu, C. L. Fu, G. W. Xu, J. R. Lian, and Y. P. Wang, Sens. Actuators, B **230**, 206 (2016).
23. S. Q. Cao, Y. Shao, Y. Wang, T. S. Wu, L. F. Zhang, Y. J. Huang, F. Zhang, C. R. Liao, J. He, and Y. P. Wang, Opt. Express **26**, 3988 (2018).
24. X. W. Shu, L. Zhang, and I. Bennion, J. Lightwave Technol. **20**, 255 (2002).
25. X. W. Shu, X. Zhu, Q. Wang, S. Jiang, W. Shi, Z. Huang, and D. Huang, Electron. Lett. **35**, 649 (1999).
26. I. Del Villar, Opt. Express **23**, 8389 (2015).
27. C. Du, Q. Wang, Y. Zhao, and S. Hu, Opt. Laser Technol. **112**, 261 (2019).
28. Q. Ling, Z. T. Gu, and K. Gao, Appl. Opt. **57**, 2693 (2018).
29. I. Del Villar, J. L. Cruz, A. B. Socorro, J. M. Corres, and I. R. Matias, Opt. Express **24**, 17680 (2016).
30. Z. Y. Liu, Y. Q. Liu, C. B. Mou, F. Zhou, and T. Y. Wang, Appl. Opt. **57**, 4756 (2018).
31. Q. Ling, Z. T. Gu, X. L. Jiang, and K. Gao, Opt. Commun. **439**, 187 (2019).
32. Z. L. Li, S. Liu, Z. Y. Bai, C. L. Fu, Y. Zhang, Z. Y. Sun, X. Y. Liu, and Y. P. Wang, Opt. Express **26**, 24114 (2018).
33. M. Zhou, Z. Zhang, L. P. Shao, S. Liu, Y. Liu, Y. Pang, Z. Y. Bai, C. L. Fu, W. Cui, and Y. P. Wang, Opt. Express **29**, 15595 (2021).
34. Y. Y. Zhao, S. Liu, J. X. Luo, Y. P. Chen, C. L. Fu, C. Xiong, Y. Wang, S. Y. Jing, Z. Y. Bai, C. L. Liao, and Y. P. Wang, J. Lightwave Technol. **38**, 2504 (2020).